Mechanism of the order–disorder phase transition, and glassy behavior in the metal-organic framework $[(CH_3)_2NH_2]Zn(HCOO)_3$

Tiglet Besara[a,b], Prashant Jain[a,b,1], Naresh S. Dalal[b,a,1], Philip L. Kuhns[a], Arneil P. Reyes[a], Harold W. Kroto[b,1], and Anthony K. Cheetham[c,1]

[a]National High Magnetic Field Laboratory, Tallahassee, FL 32310; [b]Department of Chemistry and Biochemistry, Florida State University, Tallahassee, FL 32306; and [c]Department of Materials and Metallurgy, University of Cambridge, Cambridge CB2 3QZ, United Kingdom

Contributed by Harold W. Kroto, February 14, 2011 (sent for review June 14, 2010)

Transitions associated with orientational order–disorder phenomena are found in a wide range of materials and may have a significant impact on their properties. In this work, specific heat and ^{1}H NMR measurements have been used to study the phase transition in the metal-organic framework (MOF) compound $[(CH_3)_2NH_2]Zn(HCOO)_3$. This compound, which possesses a perovskite-type architecture, undergoes a remarkable order–disorder phase transition at 156 K. The $(CH_3)_2NH_2^+$ (DMA^+) cationic moieties that are bound by hydrogen bonds to the oxygens of the formate groups (N—H···O ~ 2.9 Å) are essentially trapped inside the basic perovskite cage architecture. Above 156 K, it is the orientations of these moieties that are responsible for the disorder, as each can take up three different orientations with equal probability. Below 156 K, the DMA^+ is ordered within one of these sites, although the moiety still retains a considerable state of motion. Below 40 K, the rotational motions of the methyl groups start to freeze. As the temperature is increased from 4 K in the NMR measurements, different relaxation pathways can be observed in the temperature range approximately 65–150 K, as a result of a "memory effect." This dynamic behavior is characteristic of a glass in which multiple states possess similar energies, found here for a MOF. This conclusion is strongly supported by the specific heat data.

multiferroic | organic-inorganic solids

Metal-organic framework (MOF) compounds are extended organic–inorganic crystalline solids in well-defined geometric structures (1, 2). Because of the exciting possibility of dynamic and related behavior with advanced device applications, considerable effort is currently being devoted to creating previously undescribed MOF compounds (3, 4). We recently reported a series of multifunctional MOF compounds that simultaneously exhibit ferromagnetic and ferroelectric behavior associated with orientational ordering (5, 6). These compounds possess the perovskite structure, ABX_3, with A as the dimethylammonium cation $(CH_3)_2NH_2^+$, DMA^+; B as a divalent transition metal ion (Zn^{2+}, Mn^{2+}, Ni^{2+}, Fe^{2+}, etc.), and X as the formate ion HCO_2^- (5, 6). Because many of the inorganic perovskites are ferroelectrics, it was interesting to find these analogous MOF compounds to also exhibit ferroelectric behavior, but the microscopic mechanism of the onset of ferroelectricity and the concomitant solid/solid-phase transition was not fully understood (5, 6). A clue to the mechanism is provided by the molecular structure. X-ray studies show that $[(CH_3)_2NH_2]Zn(HCOO)_3$ (henceforth DMAZF) has the basic perovskite architecture in which the metal atoms are located at the corners of a cube and are connected via the oxygen atoms of formate linkers (Zn—O—CH—O—Zn) (Fig. 1) (6, 7). The DMA^+ cation is located in the cavity and is hydrogen-bonded to the formate frame via its amino H atoms to the formate O atoms, and—in analogy with the antiferroelectric phase transition in $NH_4H_2PO_4$—the making and breaking of the N—H···O bonds in the unit cell are the cause of the phase transition and the dipole moment dynamics (8).

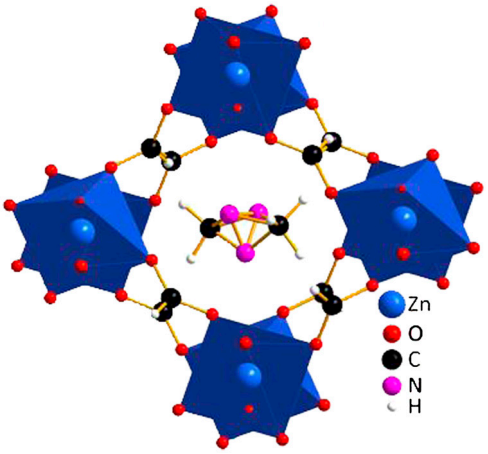

Fig. 1. Crystal structure of $[(CH_3)_2NH_2]Zn(HCOO)_3$ at room temperature. The purple spheres represent the three dynamically disordered sites for the N atom of the DMA^+ cation.

Because of the intrinsic weakness of the H bonds, the nitrogen moves between three distinct but equivalent positions at high temperatures ($T > 156$ K), due to thermally induced hindered motion. Upon cooling, the compound undergoes a phase transition as the three sites become inequivalent for a given cavity as far as the nitrogen is concerned, but not enough to freeze the motion. This conclusion is supported by a recent Raman study by Sanchez-Andujar et al. (9) on the manganese analogue of DMAZF showing that as the temperature is lowered, the NH_2 Raman peaks exhibit splittings at 100 K. Moreover, single crystal X-ray determination of the low temperature phase by these authors (9) showed that it belonged to a ferroelectric space group, a result consistent with our dielectric measurements (6). However, no measurements at temperatures close to T_c were reported (9).

In this paper, we report the results of detailed NMR and specific heat (C_p) measurements on DMAZF that show (*i*) a slowing down of the hopping motion of the caged dimethylammonium moiety, with a minimum in the ^{1}H spin-lattice relaxation time (T_1) around the phase transition; (*ii*) an unusual memory effect in the temperature dependence of T_1 at temperatures

Author contributions: P.J., N.S.D., and A.K.C. designed research; T.B., P.J., P.L.K., and A.P.R. performed research; T.B., P.J., N.S.D., P.L.K., A.P.R., A.K.C., and H.W.K. analyzed data; and T.B., P.J., N.S.D., P.L.K., A.P.R., A.K.C., and H.W.K. wrote the paper.

The authors declare no conflict of interest.

[1]To whom correspondence may be addressed. E-mail: pj05c@fsu.edu, dalal@chem.fsu.edu, kroto@chem.fsu.edu, or akc30@cam.ac.uk.

below the phase transition, implying glass-like behavior; and (*iii*) a peak in C_p/T^3 vs. T data, which corroborates the presence of a glassy phase. To the best of our knowledge, glassy behavior of a single crystalline MOF has not been reported before.

To study the motion of the DMA^+ ion in relation to the phase transition, we measured the nuclear spin-lattice relaxation time of the ^1H nuclei across the critical temperature $T_c \approx 156$ K, and over a relatively wide temperature range (4–250 K). The T_1 was used as a probe of the local order and molecular dynamics (time scale approximately $10^{-10} - 10^{-12}$ s) of the DMA^+ unit and was measured using a spectrometer available at the National High Magnetic Field Laboratory. The standard $\pi/2 - \tau - \pi/2$ saturation recovery procedure was used with a field of 6.267 T (corresponding to 266.8 MHz for protons). The observed ^1H signal was a single, broad peak, containing contributions from all the protons. The sample consisted of 20–30 submillimeter-sized single crystals, synthesized as described elsewhere (6).

Fig. 2 summarizes the behavior of the proton spin-lattice relaxation rate, T_1^{-1}, over a wide temperature range around the transition temperature, T_c. The graph has been divided into three regions (the regions depicted by Fig. 2 *A*–*C*), guided by natural breaks in the slope. In the region depicted by Fig. 2*C*, DMAZF is in the high-temperature paraelectric phase. On lowering the temperature, T_1^{-1} increases steadily and reaches a maximum around T_c, whereafter it starts to decrease as DMAZF enters the ferroelectrically ordered phase (the regions depicted in Fig. 2 *A* and *B*).

Our most significant observation from the measurements is that T_1^{-1} is multivalued in the region depicted in Fig. 2*B*. As long as the sample has not been previously cooled below 40 K, the behavior of the spin-lattice relaxation time is completely reversible over the temperature range 65–250 K in the regions depicted in Fig. 2 *B* and *C*. This is the main pathway, as denoted in Fig. 2. However, this reversibility does not hold for the sample if it is cooled below 40 K, and in such cases, T_1^{-1} follows a different path on warming. This unusual result is discussed in detail later in the paper. In the region depicted in Fig. 2*A*, T_1^{-1} follows a different curve, implying a change in the spin-lattice relaxation pathway.

Spin-lattice relaxation of protons in DMA^+ has been investigated earlier (10–12), and it is known to be caused by the modulation of different proton–proton dipolar interactions. These interactions are due to various dynamic processes of the DMA^+ group, including (10, 11) (*i*) isotropic and anisotropic tumbling of the DMA^+ group, (*ii*) n-fold reorientations of the DMA^+ group around its diad axis, (*iii*) internal rotations of the methyl groups around their threefold symmetry axes, and (*iv*) reorientations of the DMA^+ cation due to the nitrogen hopping among its three distinct positions.

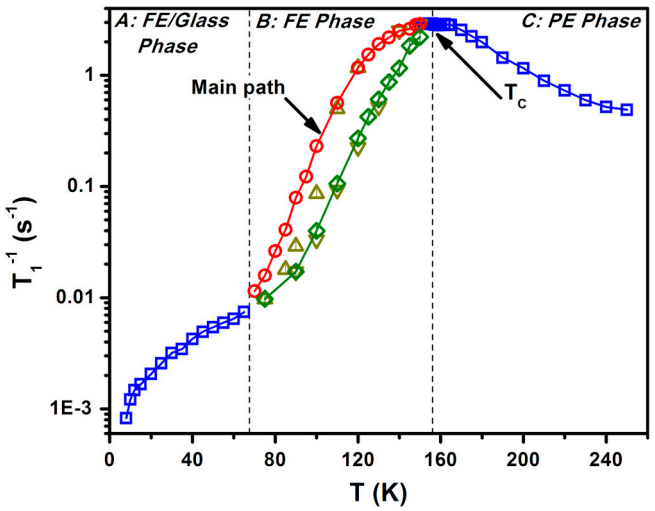

Fig. 2. Temperature dependence of the proton spin-lattice relaxation rate T_1^{-1} of DMAZF. *A*, *B*, and *C* refer to the glass, ferroelectric (FE), and paraelectric (PE) phases, respectively. The main path (circles in the region depicted in *B*) denotes the reversible temperature dependence behavior as long as the sample is not cooled below approximately 40 K. Refer to the main text for further explanation of the multivalued region depicted in *B*. Solid lines are guides to the eye, error bars are within symbols, and dashed lines emphasize the division of the relaxation rate in the three regions.

We can ignore motions (*i*) and (*ii*) as they do not preserve the symmetry of DMA^+ (10, 11) and are therefore expected to be quite hindered, taking place only at very high temperatures, higher than the range in the current study. Therefore, in the following analysis, we consider only the two processes (*iii*) and (*iv*), keeping in mind that motion (*iv*) not only involves the NH_2 motion but also the motion of the CH_3 as a group. Motion (*iii*) is expected to dominate the relaxation only at lower temperatures, well below the phase transition. Thus, the most dominant motion for the ^1H T_1 at temperatures around the phase transition is motion (*iv*). It should, however, be stressed that, because only a single relaxation time was observed, it is assumed that also spin diffusion among the various types of protons exists that actually mixes all the relaxation pathways. Therefore, the single relaxation time that is observed is a weighted average value of all relaxations.

The well-rounded maximum in T_1^{-1} (or minimum in T_1; see Fig. 3) in the close vicinity of the phase transition suggests that the hopping motion of the DMA^+ slows down smoothly at T_c, rather than showing a sudden divergence as might be expected from a complete freezing-in of a motional degree of freedom at T_c. Thus, a considerable amount of motion is retained by the DMA^+ on cooling down through the phase transition. This observation is consistent with the calculation of transition entropy using the C_p curve (vide infra).

The temperature dependence of the relaxation rate that involves the paraelectric phase (the region depicted in Fig. 2*C*), the region close to the phase transition, and the main path in the ferroelectric phase (the region depicted in Fig. 2*B*) was analyzed using the Bloembergen–Purcell–Pound formalism (13), in which the relaxation rate is related to the correlation time, τ_c, which is the characteristic time between significant fluctuations in the local magnetic field experienced by a spin due to molecular motions or reorientations of a molecule. As the relaxation rate along this path is dominated by only the two dynamic processes (*iii*) and (*iv*), we can write a simplified expression of the total relaxation rate as a sum of two relaxation rates:

$$\begin{aligned}\frac{1}{T_1} &= \frac{1}{T_1^{(1)}} + \frac{1}{T_1^{(2)}} \\ &= C_1\left(\frac{\tau_{c1}}{1+(\omega_0\tau_{c1})^2} + \frac{4\tau_{c1}}{1+(2\omega_0\tau_{c1})^2}\right) \\ &\quad + C_2\left(\frac{\tau_{c2}}{1+(\omega_0\tau_{c2})^2} + \frac{4\tau_{c2}}{1+(2\omega_0\tau_{c2})^2}\right), \end{aligned} \qquad [1]$$

where ω_0 is the ^1H resonance frequency, and C_1 and C_2 are dipolar constants containing proton–proton distances. The correlation times τ_{c1} and τ_{c2} are assumed to obey the Arrhenius law

$$\tau_{ci} = \tau_{0i}\exp(E_{ai}/\mathrm{RT}), \qquad i = 1,2, \qquad [2]$$

where τ_{0i} is the single particle correlation times and E_{ai} is the activation energies for the two processes. The C_i, τ_{0i}, and E_{ai} are treated as fit parameters.

Fig. 3 shows the inverse temperature dependence of the spin-lattice relaxation time for the aforementioned regions, along with the fit to Eqs. **1** and **2**. The yielded parameters are summarized in Table 1.

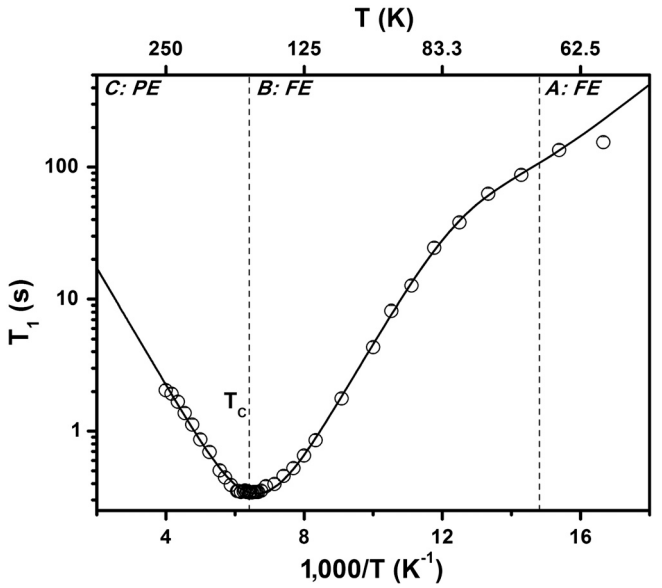

Fig. 3. Inverse temperature dependence of the proton spin-lattice relaxation time T_1 (circles). The solid line is the fit to Eqs. **1** and **2** of the data in the regions depicted in *B* and *C*. The fit was not allowed to extend into the data in the region depicted in *A*. The extension shown is an extrapolation of the fit. The dashed lines are the same as in Fig. 2.

The fit to the data yields a distinct minimum in the proximity of T_c and a less significant change in curve around approximately 68 K. An equation of the form of Eq. **1** predicts two minima in the temperature dependence of T_1, at $\omega_0\tau_{c1} \approx 0.616$ and $\omega_0\tau_{c2} \approx 0.616$. Using these expressions and the parameters in Table 1 obtained from the fit, we obtain minima at $T \approx 151 \pm 2$ K and $T \approx 75 \pm 25$ K. The first minimum is in good agreement with the phase transition at 156 K. The second minimum value has a large error as the fitting was not allowed to extend into the region depicted in Fig. 2*A*. The correlation time at the phase transition, obtained from Eq. **2** and the parameters that resulted in the minimum close to T_c (see Table 1), is $\tau_{c1} \approx (3.0 \pm 0.3) \times 10^{-10}$ s. The correlation time undergoes Arrhenius slowing down, becoming $\tau_{c1} \approx (4.7 \pm 0.3) \times 10^{-10}$ s at 10 K below T_c.

When taking into account two motions, a minimum at higher temperatures is produced by the slower of the two (12). Assuming that a more complicated equation than the one used would stretch even into the region depicted in Fig. 2*A* (neglected in the current fit) and produce a second distinct minimum at lower temperatures instead of a small change in the curve, we can assume that the minimum around T_c is produced by the slower motion. Because the hindered motion of DMA^+ is a slower motional process than that of the methyl-group internal rotation, the minimum in T_1 at temperatures close to the phase transition is ascribed to the slowing down of this DMA^+ motion. However, as was mentioned earlier, the T_1 curve is continuous through the PE → FE phase transition, which implies that even though the three nitrogen sites become inequivalent at the X-ray time scale, the motion does not freeze at the NMR time scale. This is also consistent with our entropy calculations across the phase transition (6). For a complete freezing of the three-way disordered system, the expected ΔS should have been 9.1 J/mol · K ($R \ln 3$). However, the experimental value is 1.1 J/mol · K, which supports the above model. The internal threefold rotation of the CH_3 groups freezes only below 40 K.

As the DMA^+ cations acquire dipole moment, the lattice becomes ferroelectric below 156 K, a long-range polarization order starts to set in, and the motion would be expected to be correlated rather than being thermally activated. The lack of a sharp singularity in T_1 at T_c implies that thermal activation dominates the proton dynamics in the close vicinity of the phase transition. The continuity of the proton motions is not in conflict with the X-ray data that were taken at 100 K (6), where the ferroelectric domain formation should be essentially complete.

As mentioned earlier, our most significant result is the observation of a glassy behavior. This is observed in the spin-lattice relaxation time T_1 in the ferroelectric phase that becomes multivalued over the range approximately 65 K – T_c (the region depicted in Fig. 2*B*). This behavior is linked to the cooling history of the sample. Fig. 4 displays the temperature dependence of T_1^{-1} for three different relaxation pathways, in addition to the main path, in the region depicted in Fig. 2*B*.

If the sample is not cooled below *ca.* 40 K, the relaxation pathway is completely reversible (measurements were taken both on cooling and on warming). The three additional relaxation pathways shown were all observed while raising the temperature after the sample was cooled down to about 4 K. In general, these relaxation pathways do not show a continuous curve up to the region around T_c. On the contrary, the relaxation rate undergoes sudden jumps to the main (and stable) path at unpredictable temperatures. After such a jump, further measurements of T_1 follow strictly the main reversible relaxation pathway regardless of whether the sample is cooled or warmed. Needless to say, this reversibility does not hold if the sample is again cooled below 40 K. The fact that jumps from the metastable paths to the main path are unpredictable implies that the various infrastructures attained on cooling below 40 K are very close in energy. The existence of several different local domain structures with close-lying ground states is a typical manifestation of a glassy behavior (14).

Paths for which the T_1 curve remained smooth (without jumps) all the way up to the region around the phase transition, but were distinctly different from the main relaxation pathway (one such

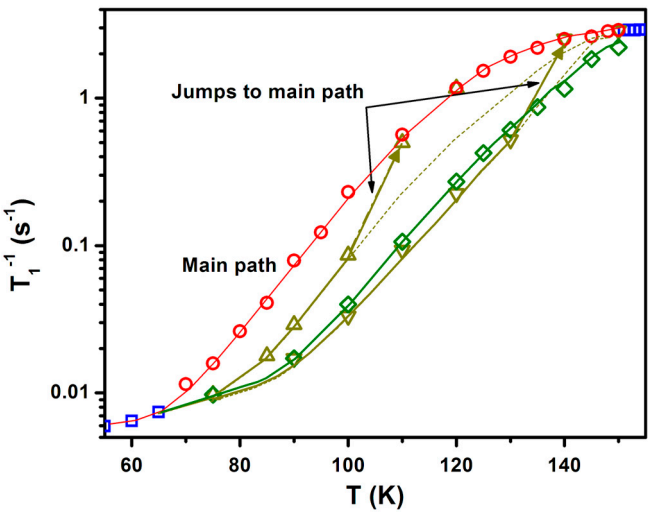

Fig. 4. Temperature dependence of the spin-lattice relaxation rate in the ferroelectric region depicted in Fig. 2*B*. Red circles represent the main path, yellow triangles represent two metastable paths, and green diamonds represent a pathway without a jump but yet distinct from the main relaxation pathway. The jumps are highlighted by arrows. The solid lines are guides to the eye. The dashed lines are the projected paths had no jumps occurred. See the main text for further explanation.

Table 1. Parameters from the fits to Eqs. 1 and 2

	E_a (kJ/mol)	τ_0 (s)	C_i (1/s^2)
$T_1^{(1)}$:	8.5 ± 0.1	4.3×10^{-13}	$(3.5 \pm 0.1) \times 10^9$
$T_1^{(2)}$:	4 ± 1	6.4×10^{-13}	$(1.1 \pm 0.1) \times 10^7$

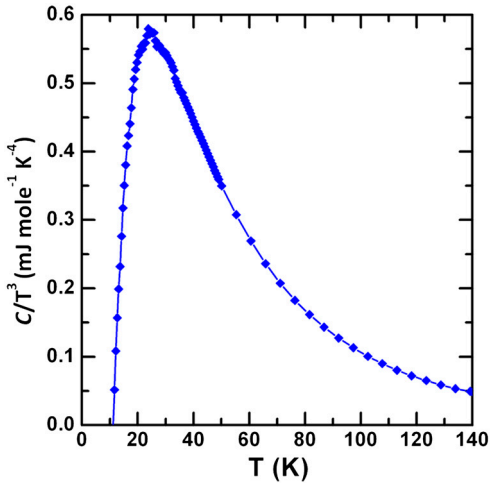

Fig. 5. Temperature dependence of low-temperature specific heat (plotted as C/T^3 vs. T) of $[(CH_3)_2NH_2]Zn(HCOO)_3$. A clear peak around 25 K is a clear manifestation of a glassy phase (see text).

path shown in Fig. 4), occurred only when the sample was cooled relatively quickly (>5 K/min) as compared to the cooling processes of the other, metastable, paths. Analyzing this relaxation pathway in a similar fashion to the main pathway, we obtain the parameters $E_a = 12.2 \pm 0.4$ kJ/mol and $\tau_0 = 4.9 \times 10^{-14}$ s. These values yield the correlation time $\tau_c \approx (5.8 \pm 2.3) \times 10^{-10}$ s at the phase transition. For this relaxation pathway, both the activation energy and the correlation time are higher, compared to the main pathway. Because T_1 depends on the local geometry, these data show that the DMA^+ moiety finds distinctly different local environments depending on the sample cooling history, again a clear signature of a glassy phase.

The spin-lattice relaxation rate, T_1^{-1}, decreases rapidly from 156 to 65 K, but the rate of decrease slows down significantly as the temperature approaches approximately 40 K. Such behavior is indicative of the opening up of a new relaxation pathway. This is because the dynamic process at these temperatures is dominated by the slowing of the methyl-group internal rotations below approximately 40 K. A similar observation has been reported by Clough and Hill (15) in methyl malonic acid and related compounds.

The T_1^{-1} curve in Fig. 2 can be decomposed into three components: one following the main relaxation pathway, a second showing a maximum around 40 K, and a third that remains essentially constant below about 10 K. The latter two pathways are analogous to the relaxation processes found in many methyl-containing solids.

The existence of a glassy state is further confirmed by our specific heat (C_p) measurements. These measurements indicated that, at low temperatures, C_p was unusually large, an observation that is a clear indication of local ordering (14). Furthermore, for glasses, the phonon heat capacity at relatively low temperatures in the range of 2–30 K is generally larger than that predicted by the Debye T^3 law (16). The excess specific heat, which is indicated by a peak in the C/T^3 vs. T curve, is generally ascribed to localized vibrations, domain wall motions of the glassy mosaic structure, and/or transverse phonon modes (17, 18). These modes are usually seen in Raman scattering as low-frequency peaks. Because these low frequencies are observed in glasses in which all types of bonding might be involved (metallic, ionic, covalent, etc.), they are recognized as fundamental features of glass dynamics (19). A number of more traditional crystalline materials also exhibit similar low temperature peaks in C/T^3 plots. Such plots have been used to explore the nature of vibrations and disorders in materials such as quartz SiO_2 and the pyrochlore $Bi_2Ti_2O_7$ (16). In the present case, the C/T^3 plot for the DMAZF also revealed a well-defined broad peak at 25 K (Fig. 5), well below its ferroelectric transition. This observation suggests that the ferroelectric ordering was not the only cooperative phenomenon involved below the transition temperature (156 K); there exists another order–disorder process, such as glass formation, at shorter length scales below 40 K. This second order–disorder process involves the freezing of the methyl-group internal rotations.

In summary, we have used ^{1}H NMR and specific heat measurements to study the motion of the central DMA^+ moiety in DMAZF crystals. The moiety exhibits unique orientational dynamics with a decrease in the motional rate with temperature, resulting in an order–disorder phase transition at 156 K. Both the long-range and the short-range ordering behavior of this crystalline MOF were probed in detail and both have shown to be related to unique motional dynamics of the DMA^+ moiety. At temperatures below 156 K, DMA^+ starts to become more ordered with decreasing temperature. Initially this involves ordering of the amine NH_2 group. Below 40 K, the internal rotations of the CH_3 groups also start to freeze, leading to multiple states with closely spaced energies. This results in a memory effect in the temperature dependence of T_1^{-1}. Local coordination environments in the framework remain unchanged as no other anomalies are observed in the specific heat measurements. However, a peak is observed at about 25 K in a C_p/T^3 vs. T plot, which is a direct manifestation of a glass phase. The present study has thus revealed a previously undescribed feature of MOF compounds—the ability to exhibit glass-like properties, akin to that shown by many inorganic perovskites.

ACKNOWLEDGMENTS. We gratefully thank Dr. John Ripmeester for highly illuminating discussions. We gratefully acknowledge financial support from European Research Council for an Advanced Investigator Award (to A.K.C.), from Florida State University (FSU) (to H.W.K. and P.J.), and from HRH Sheikh Saud bin Saqr al Qasimi (to P.J.). The work at FSU was partially supported by National Science Foundation (NSF)-Division of Materials Research (DMR) Grant 0506946. The work at National High Magnetic Field Laboratory was performed under the auspices of the NSF through the Cooperative Agreement DMR-0654118 and the State of Florida.

1. Rao CNR, Cheetham AK, Thirumurugan A (2008) Hybrid inorganic-organic materials: A new family in condensed matter physics. *J Phys Condens Matt* 20:083202.
2. Yaghi OM, et al. (2003) Reticular synthesis and the design of new materials. *Nature* 423:705–714.
3. Bureekaew S, et al. (2009) One-dimensional imidazole aggregate in aluminium porous coordination polymers with high proton conductivity. *Nat Mater* 8:831–836.
4. Férey G, Serre C (2009) Large breathing effects in three-dimensional porous hybrid matter: Facts, analyses, rules and consequences. *Chem Soc Rev* 38:1380–1399.
5. Jain P, et al. (2009) Multiferroic behavior associated with an order-disorder hydrogen bonding transition in metal-organic frameworks (MOFs) with the perovskite ABX_3 architecture. *J Am Chem Soc* 131:13625–13627.
6. Jain P, Dalal NS, Toby BH, Kroto HW, Cheetham AK (2008) Order-disorder antiferroelectric phase transition in a hybrid inorganic-organic framework with the perovskite architecture. *J Am Chem Soc* 130:10450–10451.
7. Wang X-Y, Gan L, Zhang S-W, Gao S (2004) Perovskite-like metal formates with weak ferromagnetism and as precursors to amorphous materials. *Inorg Chem* 43:4615–4625.
8. Gough SR, Ripmeester JA, Dalal NS, Reddoch AH (1979) Thermal hysteresis at the low temperature phase transition of $(NH_4)H_2PO_4$, $(NH_4)As_2PO_4$, their deuterated analogs, and of KH_2PO_4 and the effect of Cr impurity ions on the transition temperature. *J Phys Chem* 83:664–669.
9. Sanchez-Andujar M, et al. (2010) Characterization of the order-disorder dielectric transition in the hybrid organic-inorganic perovskite-like formate $Mn(HCOO)_3[(CH_3)_2NH_2]$. *Inorg Chem* 49:1510–1516.
10. Jagadeesh B, Rajan PK, Venu K, Sastry VSS (1994) Order-disorder phase transition and dimethyl ammonium group dynamics in $[(CH_3)_2NH_2]_3Sb_2Cl_9$-proton NMR study. *Solid State Commun* 91:843–847.
11. Venu K, Sastry VSS (1993) Proton spin lattice relaxation in the dimethylammonium group. *Z Naturforsch* 48A:713–719.
12. Dolinšek J, et al. (1999) ^{1}H and ^{27}Al NMR study of the ferroelectric transition in dimethylammonium aluminum sulphate hexahydrate $(CH_3)_2NH_2Al(SO_4)_2 \cdot 6H_2O$. *Phys Rev B* 59:3460–3467.
13. Bloembergen N, Purcell EM, Pound RV (1948) Relaxation effects in nuclear magnetic resonance absorption. *Phys Rev* 73:679–712.

14. Angell CA (1995) Formation of glasses from liquids and biopolymers. *Science* 267:1924–1935.
15. Clough S, Hill JR (1974) Temperature dependence of methyl group tunnelling rotation frequency. *J Phys C* 7:L20–L21.
16. Melot BC, et al. (2009) Large low-temperature specific heat in pyrochlore $Bi_2Ti_2O_7$. *Phys Rev B* 79:224111.
17. Lubchenko V, Wolynes PG (2003) The origin of the boson peak and thermal conductivity plateau in low-temperature glasses. *Proc Natl Acad Sci USA* 100:1515–1518.
18. Shintani H, Tanaka H (2008) Universal link between the boson peak and transverse phonons in glass. *Nat Mater* 7:870–877.
19. Safarik DJ, Schwarz RB, Hundley MF (2006) Similarities in the C_p/T^3 peaks in amorphous and crystalline metals. *Phys Rev Lett* 96:195902.